



Validation of western and eastern Pacific rainfall estimates from the TRMM PR using a radiative transfer model

S. Shige,¹ T. Watanabe,¹ H. Sasaki,¹ T. Kubota,^{1,2} S. Kida,¹ and K. Okamoto¹

Received 18 May 2007; revised 7 March 2008; accepted 24 March 2008; published 8 August 2008.

[1] Rainfall estimates from the Tropical Rainfall Measuring Mission (TRMM) Precipitation Radar (PR) facility algorithm over the eastern Pacific are lower than those from the TRMM Microwave Imager (TMI) facility algorithm and a PR-consistent advanced microwave radiometer algorithm, while they are in good agreement over the western Pacific. We investigate the consistency between TMI-observed brightness temperatures (*T*_B) for the 19 GHz channel and those simulated from the PR rainfall estimates using a radiative transfer model. Discrepancies between observed *T*_B and simulated *T*_B from the PR are larger for the eastern Pacific than for the western Pacific, indicating that PR underestimates rainfall over the eastern Pacific. It is hypothesized that drop size distributions (DSDs) in the eastern Pacific have stronger maritimicity (i.e., more small to medium sized raindrops) than the initial DSD model of the PR algorithm, representative of the “data-rich” western Pacific, leading to underestimation of rain by the PR. Differences in the adjustable parameter of the PR algorithm, implying changes in the DSD, and the vertical structure of PR-observed reflectivity over the western and eastern Pacific support the hypothesis.

Citation: Shige, S., T. Watanabe, H. Sasaki, T. Kubota, S. Kida, and K. Okamoto (2008), Validation of western and eastern Pacific rainfall estimates from the TRMM PR using a radiative transfer model, *J. Geophys. Res.*, 113, D15116, doi:10.1029/2007JD009002.

1. Introduction

[2] The Tropical Rainfall Measuring Mission (TRMM) [Simpson *et al.*, 1988, 1996; Kummerow *et al.*, 2000] is the first satellite to carry both active and passive microwave sensors for measuring precipitation, leading to significantly better and more consistent rainfall estimates throughout the Tropics. The TRMM Precipitation Radar (PR) is the first space-borne precipitation radar and provides height information based upon the time delay of the precipitation-backscattered return power and allows vertical profiles of precipitation to be obtained directly over the global Tropics [Kozu *et al.*, 2001; Okamoto, 2003]. The TRMM Microwave Imager (TMI) measures radiances that are the end product of the integrated effects of electromagnetic absorption/emission and scattering through a precipitating cloud along the sensor viewpath.

[3] By comparison, the more direct measurement of hydrometeors by the PR seems to have less uncertainty. The PR estimates, therefore, have been commonly used as a reference to validate rainfall estimates from passive microwave imagers [e.g., Yang *et al.*, 2006; Kubota *et al.*, 2007]. The PR operates at a single frequency of 13.8 GHz so that the PR2A25 algorithm corrects the attenuation in the measured radar reflectivity factor Z_m

and estimates the attenuation-corrected radar reflectivity factor Z_e [Iguchi and Meneghini, 1994; Iguchi *et al.*, 2000]. The attenuation correction is based on a hybrid method that provides a smooth transition between the Hitschfeld–Bordan [Hitschfeld and Bordan, 1954] method, which performs well at low attenuations, and the surface reference technique [Meneghini *et al.*, 2000], for which the relative error decreases with increasing path-integrated attenuation (PIA). This method is termed the “ α -adjustment” method [Iguchi and Meneghini, 1994]. The coefficient α in the $k_p - Z_e$ relationship.

$$k_p = \alpha Z_e^\beta \quad (1)$$

is adjusted in such a way that the PIA estimated from the H-B method matches the SRT estimate of PIA where k_p is the specific attenuation due to precipitation. Although specific attenuation in precipitation at TRMM PR frequencies is predominantly due to absorption and is roughly proportional to the volume of rain, the reflectivity is proportional to the sixth power of raindrop diameter, and thus sensitive to variant properties of the drop size distribution (DSD), which is the greatest weakness of the PR.

[4] The differences between PR2A25 [Iguchi *et al.*, 2000; Iguchi, 2007] and TMI2A12 [Kummerow *et al.*, 2001; Olson *et al.*, 2006] standard rainfall products over the eastern Pacific are well known [Berg *et al.*, 2002, 2006]. The most common method of verifying satellite-retrieved rain estimates is to directly compare to ground validation measurements (ground truth) derived from rain gauge net-

¹Department of Aerospace Engineering, Osaka Prefecture University, Sakai, Osaka, Japan.

²Japan Science and Technology Agency, Kawaguchi, Saitama, Japan.

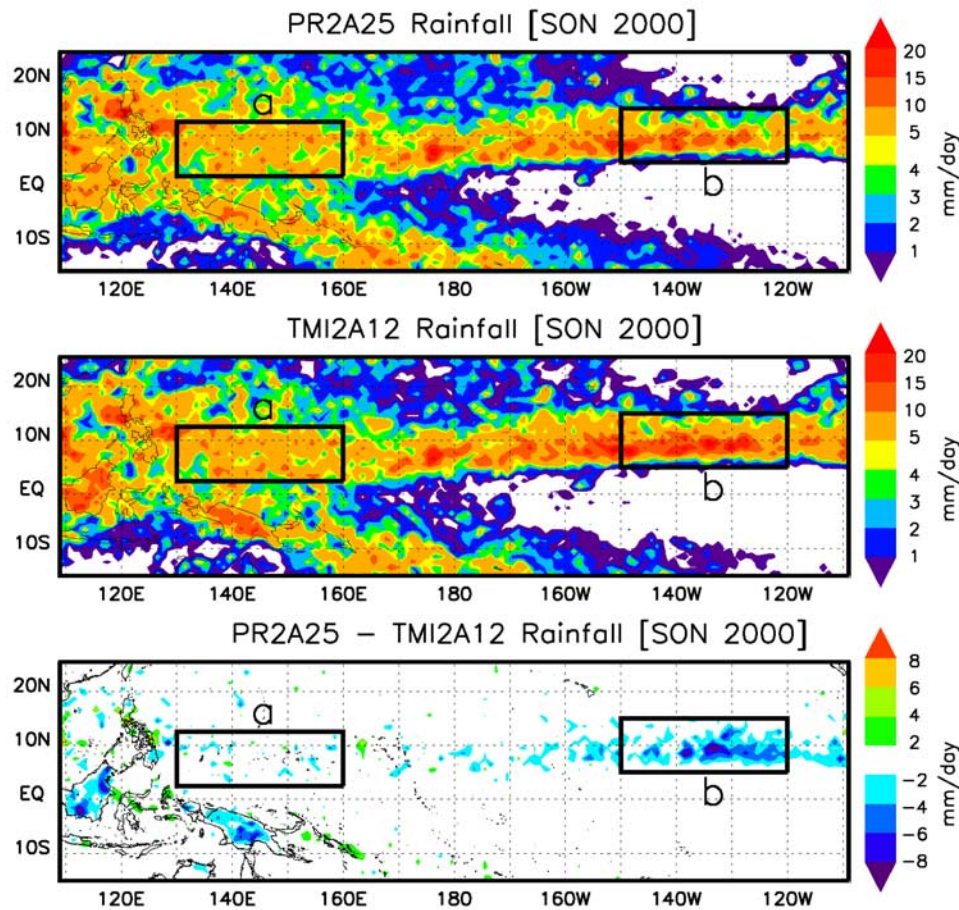


Figure 1. Rainfall estimates from version 6 of (top) PR2A25 and (middle) TMI2A12 retrieval algorithms for the 3-month period from SON 2000. (bottom) Rainfall difference map between version 6 of the PR2A25 and TMI2A12 retrieval algorithms for the 3-month period from SON 2000. The maps were created from the 3G68 data set, which matches the instantaneous PR2A25 and TMI2A12 estimates on a $0.5^\circ \times 0.5^\circ$ grid. Boxes indicating the locations of (a) the selected western Pacific (2.5° – 12.5° N, 130° – 160° E) and (b) the eastern Pacific (5.0° – 15° N, 120° – 150° W) are also shown.

works, ground weather radar, or a combination of the two. However, precipitation has been poorly observed over the oceans owing to sparse observations. In particular, very few in situ measurements of rainfall are available for the eastern Pacific intertropical convergence zone (ITCZ) [Janowiak *et al.*, 1995]. It has also proven to be extremely difficult to make accurate ground-based measurements of precipitation from ships [e.g., Yuter and Parker, 2001]. Thus we must rely on indirect strategies for validation. Smith and Hollis [2003] evaluated and validated the TRMM facility rain profile algorithms by an algorithm-to-algorithm intercomparison analysis in the context of physical hypothesis testing. Berg *et al.* [2006] have attempted to identify globally observable physical variables that can be used as a proxy for PR/TMI differences and, by association, the corresponding regime-dependent cloud properties. Shige *et al.* [2006, hereinafter SAL] investigated the consistency between TMI-observed brightness temperatures (hereinafter *TBs*) and those simulated from PR2A25 V5 and V6 rain profiles for the ITCZ precipitation systems during the 1997/1998 El Niño event when there were large discrepancies between the TRMM version-5 rainfall products [Robertson

et al., 2003]. Simulated *TBs* at 10 GHz from PR V6 have better agreement with observed *TBs* than do *TBs* from PR V5, implying algorithm improvements. However, discrepancies at 19 GHz suggest that uncertainty in the assumed DSD still remains in PR V6.

[5] In this study, the previous work of SAL is extended to validate PR2A25 V6 over the western and eastern Pacific during a normal year using independent TMI-observed *TB* data.

2. Approach

[6] The present study uses the same approach as that shown in Figure 1 of SAL. The difference is that SAL examined the consistency between TMI-observed *TBs* and those simulated at 10 and 19 GHz, while this work examines only the consistency at 19 GHz. Because the population of heavy rainfall is very small during a normal year, comparing radiative characteristics at 10 GHz, which implies validating heavy rain, is meaningless. While SAL investigated the consistency between TMI-observed *TBs* and those simulated from PR2A25 V6 and TMI2A12 V6 rain profiles, this study only investigates the consistency

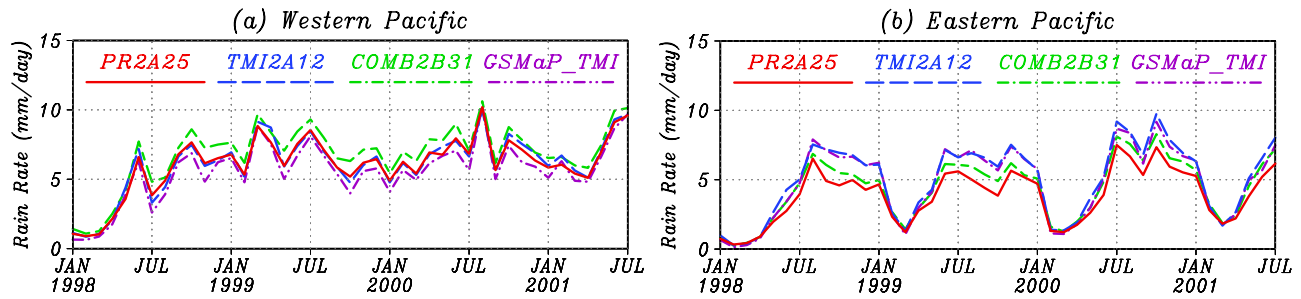


Figure 2. Time series of monthly mean rainfall estimates from PR2A25, TMI2A12, COMB2B31 and GSMaP_TMI for (a) the western Pacific and (b) the eastern Pacific.

between TMI-observed TBs and those simulated from PR2A25 V6 rain profiles. It was shown by SAL that the 19 GHz channel significantly contributes to the rain retrieval of the TMI2A12 algorithm, and thus comparing TMI-observed TBs to those simulated from TMI2A12 V6 rain profiles is meaningless as a validation.

[7] The four-stream plane-parallel radiative transfer model (RTM) developed by Liu [1998] is used to calculate TBs . RTM calculations are performed for each $4 \text{ km} \times 4 \text{ km}$ PR pixel before the TBs are averaged for the radiometer field of view (FOV). The antenna pattern for the 19 GHz channel is approximated by a Gaussian weighting function with the same 3-dB beam width as the actual antenna pattern, taking into account the rotation of the TMI antenna. All radiance slant paths through the three-dimensional domain are considered independently. Horizontal displacement in the direction of sight is caused by signal contributions from layers other than those near the surface that are projected onto the footprint of the observation [Bauer *et al.*, 1998]. Thus at frequencies (37 and 85 GHz) sensitive to ice particle scattering the projection effect is most significant. On the other hand, the 19 GHz channel is sensitive to rainfall at lower-levels, and the FOV for the 19 GHz channel is larger than those of higher frequency channels. Hence the slant-path approximation produces only slightly higher simulated TBs from PR2A25 rain profiles, resulting in better agreement with TMI-observed TBs .

[8] Column water vapor (CWV), liquid water path (LWP), sea surface wind, and sea surface temperature (SST) are adopted from the TMI products provided by Remote Sensing Systems, while mean atmospheric temperature from the 6-hourly ERA40 reanalysis data with minimum time difference with the TRMM observations is employed. For PR data, we use two DSD models of a gamma distribution corresponding to convective and stratiform rain assumed in PR algorithm [Iguchi *et al.*, 2000]. A change in the DSD due to a variation in α accommodating the SRT estimate of PIA is also taken into account. For PR stratiform rain profiles with a bright band, the melting-layer parameterization of Klaassen [1990] is used, following Kim *et al.* [2004]. Details on the simulation setting were provided in SAL and Sasaki *et al.* [2007]. Sasaki *et al.* [2007] showed the effects of using different DSD models on simulated brightness temperature at 19 GHz are negligibly small, while those at 10 GHz are considerably large, which is consistent with the results from Coppens and Haddad [2000] that show the effect of varying the DSD is smallest

between 16 and 19 GHz. Thus validation using the simulation of 19 GHz radiances from PR rain profiles, which are mainly a function of water content, is robust.

[9] For comparison, the emission index (EI) is defined as $1 - P$ and used instead of TB to isolate the microwave signal due to precipitation particles [Greco *et al.*, 2004]. Here, P is the normalized polarization difference [Petty, 1994] given by

$$P = \frac{TB_V - TB_H}{TB_{V,clear} - TB_{H,clear}}, \quad (2)$$

where TB_V and TB_H are the vertically and horizontally polarized brightness temperatures and $TB_{V,clear}$ and $TB_{H,clear}$ are background brightness temperatures in the absence of cloud or precipitation. For the observed P , the background brightness temperatures are estimated following the method of TMI 2A12 V6 [Olson *et al.*, 2006]. For the simulated P , the background brightness temperatures are calculated with all cloud and precipitation water contents set to zero. The EI is zero for a zero rain rate and increases with rain rate.

3. Results

[10] Figure 1 shows a comparison of rainfalls from version 6 of the TRMM PR2A25 and TMI2A12 standard products over the Pacific for the period from September to November (SON) 2000. Two regions in the ITCZ were selected for comparison. One region is over the western Pacific warm pool and the other encompasses the region of maximum differences between PR and TMI estimates over the eastern Pacific as shown in Figure 1. Both selected regions are of the same dimensions and are over ocean-only areas in the ITCZ. The figure clearly shows large differences in eastern Pacific ITCZ rainfall, with a negative bias for PR estimates relative to the TMI estimates.

[11] Time series are shown in Figure 2, indicating there are larger biases for the selected eastern Pacific than for the selected western Pacific during the period from January 1998 through July 2001. Increasing bias was found after August 2001 when the TRMM satellite was boosted from 350 km to 402.5 km to conserve fuel. The effects of the boost on an active sensor, PR, should be larger than those on a passive sensor, TMI, but an investigation is beyond the scope of the study. The differences between PR and TMI estimates for October 2000 are 6% over the western Pacific and 29% over the eastern Pacific, respectively. The difference over the eastern Pacific is larger than the difference

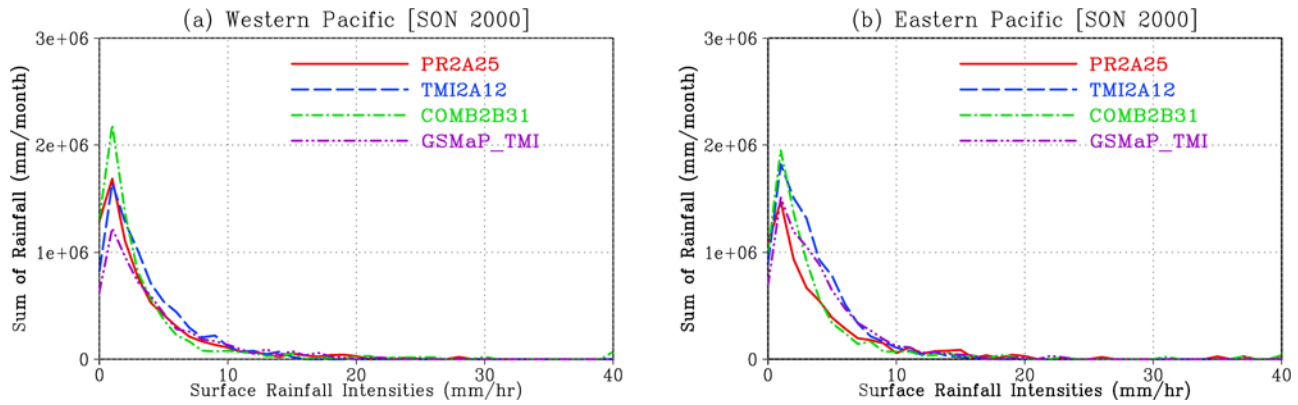


Figure 3. Histogram showing sum of rain rates at 0.5° resolution from PR2A25, TMI2A12, COMB2B31 and GSMaP_TMI for SON 2000 over (a) the western Pacific and (b) the eastern Pacific.

over the central Pacific during the 1997/1998 El Niño (February 1998) event, which was found to be with 11% by SAL. TMI2A12 estimates greater rainfall over the eastern Pacific than over the western Pacific, while PR2A25 estimates slightly less rainfall over the eastern Pacific than over the western Pacific. Such discrepancies in west-east gradients of rainfall are crucial for ENSO indices based on the zonal gradient of rainfall in the equatorial Pacific [Curtis and Adler, 2000].

[12] The basis of the TMI 2A12 algorithm is based on a “Bayesian” framework, in which retrieved precipitation is constructed from those cloud-resolving model (CRM)-generated profiles that are radiatively consistent with the observation [Kummerow *et al.*, 1996, 2001]. Although the cloud-radiative model database supporting the TMI2A12 V6 algorithm has been expanded, the database consists of only six simulations [Olson *et al.*, 2006, Table 2]. The shallower convective events common to the eastern Pacific may not be represented in the cloud-radiative model database supporting the TMI2A12 V6 algorithm, leading to an overestimation of rain in the eastern Pacific.

[13] As references, time series of rainfall estimates using two other algorithms are also shown in Figure 2. One is the TRMM combined PR and TMI 2B31 (hereinafter COMB2B31) algorithm [Haddad *et al.*, 1997]. Over both the western and eastern Pacific, COMB2B31 estimates are larger than PR2A25 estimates. Although theoretically the radar-radiometer estimates may lead to better results than the radar-only estimates, PR2A25 products rather than COMB2B31 products have been used in a great many studies. One possible limitation of the COMB2B31 algorithm, which was designed primarily with operational goals for TRMM, resides in the fact that the *TBs* associated with a given reflectivity profile are not explicitly calculated using physical models, but are estimated based on a priori statistical relationships. Consequently, the errors in the estimated *TBs* may be larger than those derived from a physical model.

[14] The other algorithm is the Global Satellite Mapping Project (GSMaP) rain-retrieval algorithm [Kubota *et al.*, 2007], which is a PR-consistent advanced microwave radiometer algorithm based on the study by Aonashi and Liu [2000]. The basic idea of the GSMaP algorithm is to find the optimal rainfall that gives RTM FOV-averaged *TBs* that

fit best the observed *TBs*. Using RTM, lookup tables showing the relationship between rainfall rates and *TBs* were computed daily in $5^\circ \times 5^\circ$ latitude-longitude boxes, with atmospheric variables (freezing level height, temperature, relative humidity, surface winds and surface temperature) given by the Japan Meteorological Agency (JMA) Global Analysis (GANAL). RTM calculations use a tri-monthly database of precipitation types and profiles in $2.5 \times 2.5^\circ$ latitude-longitude boxes derived from the PR2A25 data, together with the melting-layer model used in the PR2A25 algorithm. Thus compared with the supporting databases of the TMI2A12 algorithm, those of the GSMaP algorithm are more consistent with naturally occurring profiles at the time/location where the algorithm is applied. Here, the current version “4.8.4” of the GSMaP algorithm for TMI (hereinafter GSMaP_TMI) was used. In spite of differences in the supporting databases and the process of retrievals from *TBs*, the GSMaP_TMI estimates are similar to the TMI2A12 estimates in that they are larger than PR estimates over the eastern Pacific, while they are in good agreement over the western Pacific.

[15] The histogram in Figure 3 shows the sum of rain rates during SON 2000 from PR2A25, TMI2A12, COMB2B31 and GSMaP_TMI at 0.5° resolution. Though the TMI2A12 estimates are smaller than PR2A25 estimates at very light rain rates ($0 \text{ mm h}^{-1} < R \leq 1 \text{ mm h}^{-1}$) and are slightly larger than PR2A25 estimates at light-to-moderate rain rates ($3 \text{ mm h}^{-1} < R \leq 10 \text{ mm h}^{-1}$), the histogram shows good agreement between TMI2A12 and PR2A25 over the western Pacific. The difference at very light rain rates is probably due to the sensitivity of the TMI2A12 algorithm, which is limited primarily by the difficulty of distinguishing precipitating from nonprecipitating clouds. On the other hand, the sum of rain rates in the range $2 \text{ mm h}^{-1} < R \leq 10 \text{ mm h}^{-1}$ is much larger for TMI2A12 than for PR2A25 over the eastern Pacific. While the difference in the sum of rain rates in the range $2 \text{ mm h}^{-1} < R \leq 10 \text{ mm h}^{-1}$ between TMI2A12 and PR2A25 is $1453.62 \text{ mm month}^{-1}$ over the western Pacific, the difference is $3829.17 \text{ mm month}^{-1}$ over the eastern Pacific, resulting in variability of the biases across the Pacific. COMB2B31 estimates are larger than PR2A25 estimates below 5 mm h^{-1} , while COMB2B31 estimates are smaller than PR2A25 estimates above 5 mm h^{-1} , over

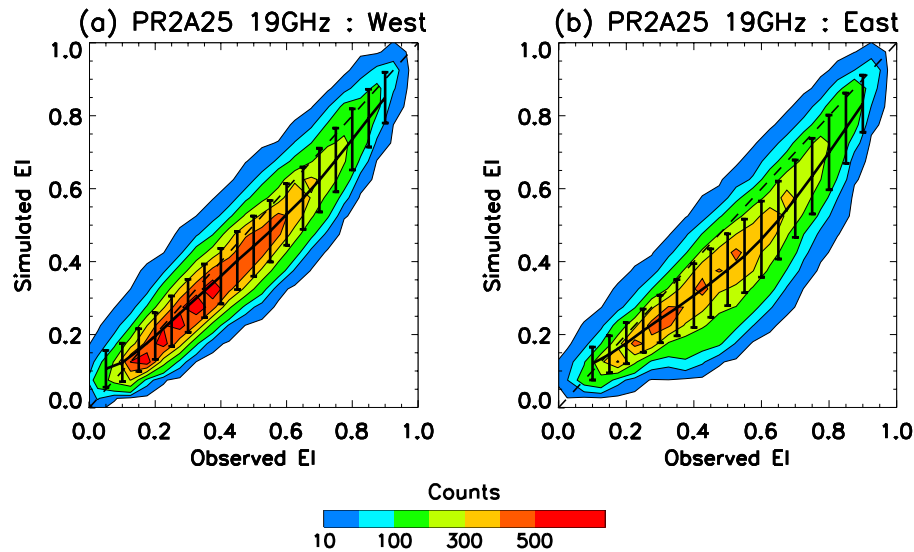


Figure 4. Frequency plots of the 19 GHz emission indexes (EIs) simulated from PR2A25 rain profiles for (a) the western Pacific and (b) the eastern Pacific against corresponding TMI-observed 19 GHz EIs. The average (solid line) and standard deviation (error bars) of simulated EI for each histogram bin along the horizontal line are plotted. The dashed lines are the 1:1 lines.

both the western and eastern Pacific, perhaps reflecting that the *TBs* associated with a given reflectivity profile are estimated based on a priori statistical relationships. The GSMaP_TMI estimates are in very good agreement with the PR2A25 estimates over the western Pacific, except for below 2 mm hr^{-1} . The larger negative bias below 2 mm hr^{-1} in the GSMaP_TMI estimates than in the TMI2A12 estimates may be caused by the rain/no-rain threshold being 0.5 kg m^{-2} of cloud water in the GSMaP_TMI algorithm [Aonashi and Liu, 2000], while the threshold is 0.3 kg m^{-2} of cloud water in the TMI2A12 algorithm [Berg et al., 2006]. On the other hand, the sum of rain rates in the range $3 \text{ mm h}^{-1} < R \leq 10 \text{ mm h}^{-1}$ is much larger for GSMaP_TMI than for PR2A25 over the eastern Pacific. While the difference in the sum of rain rates in the range $3 \text{ mm h}^{-1} < R \leq 10 \text{ mm h}^{-1}$ between GSMaP_TMI and PR2A25 is $52.39 \text{ mm month}^{-1}$ over the western Pacific, that it is $2360.18 \text{ mm month}^{-1}$ over the eastern Pacific. Although the database of the GSMaP algorithm is more consistent with PR2A25 rain profiles than is the TMI2A12 algorithm database, a large bias is still found over the eastern Pacific, which motivates us to validate the PR2A25 estimates using a RTM.

[16] The procedures described in the previous section were applied to the 3 months (SON 2000) of TRMM data, over the selected western and eastern Pacific regions. The numbers of TRMM orbits used in this study were 770 and 776 for the western and eastern Pacific, respectively. Only the TMI footprints for each channels of which 80% are covered with PR rain pixels were analyzed. Frequency plots of the 19-GHz EIs (hereafter *EI19s*) simulated from PR2A25 rain profiles against corresponding TMI-observed *EI19s* for the selected western and eastern Pacific regions are presented in Figures 4a and 4b, respectively. The simulated *EI19s* from PR2A25 are lower than the observed *EI19s* over the western Pacific. Similar discrepancies have been found for precipitation systems over the central Pacific

during the 1997/1998 El Niño event by SAL. Nevertheless, the simulated *EI19s* from PR2A25 over the western Pacific have much better agreement with the observed ones than those over the eastern Pacific do. The simulated *EI19s* from PR2A25 are significantly lower than the observed *EI19s* over the eastern Pacific, especially for the low-to-medium range (smaller attenuation), resulting in an upward concave shape with respect to the observed *EI19s*. This indicates that PR2A25 underestimates rainfall over the eastern Pacific.

[17] Iguchi et al. [2000] noted the weight in the α -adjustment procedure of the PR2A25 algorithm shifts toward the SRT when attenuation is large. In such cases, the initial value of α assumed in the PR2A25 algorithm has little effect on the final Z_e near the surface, because it is essentially determined by the measured Z_m and the PIA at the surface. As a result, the a and b coefficients of the radar reflectivity–rainfall rate (Z – R) relation $R = aZ^b$ are only weakly dependent on the initial values. When attenuation is small, however, the SRT perturbs the initial choices of a and b only slightly. Therefore inappropriate selection of the initial DSD model is responsible for the underestimation of rain in the low-to-medium range.

[18] The initial DSD models used in PR2A25, made from a collection of Z – R relations measured near the ocean from widely distributed locations around the world, were representative of “maritime” distributions. Bringi et al. [2003] found “maritime-like” and “continental-like” clusters of DSD parameters by analyzing polarimetric radar and disdrometer data. “Maritime-like” DSDs are characterized by a higher concentration of smaller sized drops, while “continental-like” DSDs are characterized by a lower concentration of larger sized drops. Rosenfeld and Ulbrich [2003] indicated that rainfall rate increases for a given reflectivity with increasing maritimity of the clouds, by a factor of more than three (see their Figure 10.5), which is the manifestation of major differences in the DSDs for maritime and continental clouds. The collection of Z – R relations, from which

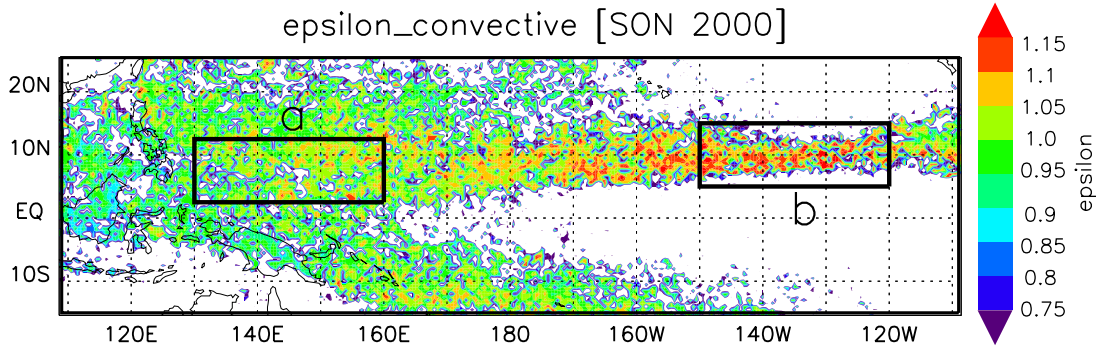


Figure 5. Convective ϵ for SON 2000 obtained from PR3A25. Grids have 0.5° spatial resolution and are monthly composites of PR2A25.

the initial DSD models used in PR2A25 were made, includes $Z-R$ relations from the “data-rich” western Pacific [Stout and Mueller, 1968; Tokay and Short, 1996], but not those from the “data-poor” eastern Pacific. Thus it is hypothesized that the DSDs of rainfall over the eastern Pacific have stronger maritimity (i.e., more small to medium sized raindrops) than does the initial DSD model of PR2A25, leading to underestimation of the rain by the PR2A25 algorithm when the SRT perturbs the initial DSD model only slightly.

[19] Iguchi [2007] noted that all variations in the $k_p - Z_e$ relationship (equation (1)) in PR2A25 are included in the variation of α as

$$k_p(r) = \epsilon(DSD)\alpha_0(r)Z_e^{\beta_0}(r) \quad (3)$$

where β_0 is assumed to be independent of range r . The variation in $\alpha_0(r)$ with r includes changes due to the phase-state difference, temperature difference, and rain type difference. The variation in α due to the changes in the DSD is taken into account by the adjustable factor $\epsilon(DSD)$. A value of ϵ less than unity implies more large raindrops and fewer small drops for the same rainfall rate, while a value of ϵ greater than unity implies fewer large raindrops and more small drops.

[20] Chandrasekhar et al. [2005] demonstrated the DSD parameters estimated from ϵ obtained from PR2A25 are in fairly good agreement with DSD retrieval from coincident dual-polarization ground data over Florida and Brazil. They suggested that similar comparisons over ocean would be better, because the SRT is inaccurate over land but much more accurate over ocean [Meneghini et al., 2000]. Figure 5 shows a map of ϵ for SON 2000 obtained from PR3A25, 0.5° spatial resolution monthly composite of PR2A25 data. Because the α -adjustment procedure based on the SRT is more useful for large attenuation scenarios, ϵ for convective rain is shown. It can be seen that ϵ over the eastern Pacific is larger than unity and ϵ over the western Pacific. This supports the hypothesis that the DSDs of rainfall over the eastern Pacific have stronger maritimity than do the initial DSD model of PR2A25 and DSDs of rainfall over the western Pacific.

[21] The RTM calculations at 19 GHz are not sensitive to the DSD assumptions, but those at 10 GHz are very sensitive [Coppens and Haddad, 2000; Sasaki et al.,

2007]. Coppens and Haddad [2000] showed larger-mean-diameter DSDs (such as the Marshall and Palmer’s [1948] distribution (hereinafter MP) and the logarithmic [Feingold and Levin, 1986]) produce higher TBs at 10 GHz, whereas smaller-mean-diameter DSDs (such as that of Sekhon and Srivastava [1971] and to a lesser extent that of Willis and Tattelman [1989]) produce lower TBs at 10 GHz. Sasaki et al. [2007] showed that MP produces TBs at 10 GHz simulated from PR2A25 rain profiles that are higher than TMI-observed TBs for the ITCZ precipitation systems during the 1997/1998 El Niño event, whereas the PR DSD models (gamma distribution) produce TBs at 10 GHz lower than TMI-observed TBs as shown by SAL. This is because MP assumes there are more large drops than does a gamma distribution with a negative shape parameter, which is downwardly concave. From the dependence of RTM calculations on the DSD, we expect rain retrievals with larger-diameter DSDs to estimate lower rain rates for a given brightness temperature than rain retrievals with smaller-diameter DSDs. In fact, the version “4.7.2” of the GSMaP algorithm using MP estimates lower rain rates over ocean than the current version “4.8.4” using a gamma distribution with negative shape parameter constructed from the ϵ database obtained from PR2A25 (Kozu et al., manuscript in preparation, 2008). Although it is possible that TMI2A12 overestimates rain rates over the eastern Pacific due to factors such as rain detection problems, any overestimation will not be due to its DSD assumption (MP).

4. Discussions

[22] To support the hypothesis that the DSDs of rainfall over the eastern Pacific have stronger maritimity than those over the western Pacific, we examined differences in the vertical structure of precipitation between the western and eastern Pacific. Here, we used contoured-frequency-by-altitude diagrams (CFADs [Yuter and Houze, 1995]) of PR2A25 V6 estimated Z_e for convective rain and stratiform rain (Figure 6).

[23] Noticeable differences in convective distributions between the western and eastern Pacific occur at low levels. The shallow convective mode extending up to ~ 3 km with low (≥ 25 dBZ) radar reflectivity is evident for the eastern Pacific (Figure 6b), while it is less evident in the western Pacific (Figure 6a). This mode is representative of warm

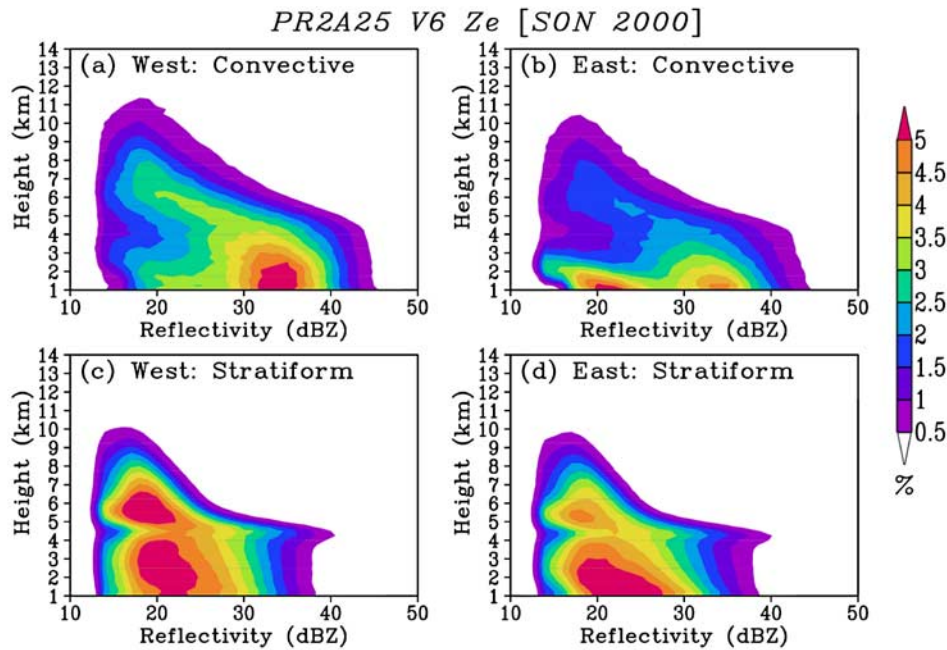


Figure 6. Contoured-frequency-by-altitude diagrams (CFADs) of PR2A25 attenuation-corrected radar reflectivity Z_e (dBZ) for convective rain over (a) the western Pacific and (b) the eastern Pacific and for stratiform rain over (c) the western Pacific and (d) the eastern Pacific for SON 2000. The bin size is 1 dBZ.

rain and includes shallow, isolated echoes, which have been reclassified as convective in V6 of the TRMM PR rain-type classification algorithm (2A23) [Awaka *et al.*, 2007] after a suggestion by Schumacher and Houze [2003]. Previous studies have noted larger populations of shallow convection over ocean than over land [e.g., Short and Nakamura, 2000; Takayabu, 2002]. Thus larger populations of shallow convection in the eastern Pacific suggest stronger maritimity of convection over the eastern Pacific than that over the western Pacific. The difference in populations of shallow convection results in differences in the shape of convective heating and drying profiles between the western and eastern Pacific estimated from TRMM PR data [Shige *et al.*, 2007, 2008].

[24] The deep convective mode possesses high (≥ 25 dBZ) radar reflectivity at low-levels and extends to greater heights over the western and eastern Pacific. Even for the deep convective mode, there are important differences in the distributions for the western and eastern Pacific. Zipser and Lutz [1994] showed that the maritime vertical profile of radar reflectivity has a maximum reflectivity at the lowest level and a very rapid decrease in reflectivity with height beginning just above the freezing level, while the continental profiles exhibit maximum reflectivity somewhat above the surface and have a gradual decrease in reflectivity with height above the freezing level. The profiles over the western Pacific have a very rapid decrease in reflectivity with height beginning just above the freezing level, similar to the maritime vertical profiles examined by Zipser and Lutz [1994]. On the other hand, the profiles over the eastern Pacific have maximum reflectivity at levels lower than those for which there is maximum reflectivity over the western

Pacific and a very rapid decrease in reflectivity with height beginning well below the freezing level.

[25] Zipser and Lutz [1994] hypothesized that the larger negative vertical gradient of reflectivity above the freezing level for the maritime profile than for the continental profile is a direct result of the characteristically weaker updrafts observed in maritime clouds than in continental clouds, which is consistent with the scarcity of lightning discharges in maritime clouds. The rapid decrease in reflectivity with height beginning well below the freezing level over the eastern Pacific suggests weaker updrafts over the eastern Pacific than over the western Pacific. Weaker updrafts help promote growth by coalescence by giving droplets more time to interact and advect less cloud water available for growth of ice hydrometeors aloft, leading to DSDs with small median drop diameters [Rosenfeld and Ulbrich, 2003].

[26] The stratiform distributions (Figures 6c and 6d) show a reflectivity enhancement near the melting level (near 5 km) associated with the radar bright-band. Significant differences in stratiform distributions between the western and eastern Pacific occur above the melting level. The CFADs of the eastern Pacific have a less probable occurrence of 20 dBZ compared with the western Pacific. Similar to convection, this indicates the development of weak ice precipitation in the eastern Pacific.

[27] The convective-stratiform classification of the DSD is taken into account by the PR2A25 algorithm, where the same Z_e translates to smaller R in stratiform rain compared with convective rain. This is based on the observation by Tokay and Short [1996] who found that stratiform rain contains more large raindrops and fewer small to medium raindrops than does convective rain using surface-based

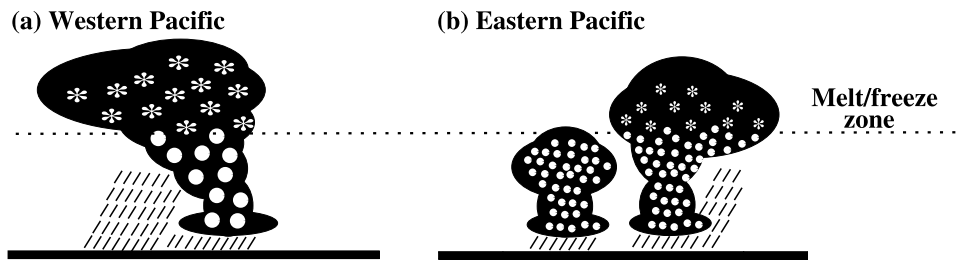


Figure 7. Schematic illustration of precipitation features over the (a) western and (b) eastern Pacific. The smaller sizes of asterisks and dots for precipitation features over the (a) western and (b) eastern Pacific. The smaller sizes of asterisks and dots for precipitation features over the eastern Pacific compared with those over the western Pacific indicate DSDs with smaller median diameters.

observations over the western Pacific. It should be noted that shallow, isolated echoes were classified as stratiform rain in V5 of the TRMM PR rain-type classification algorithm, which led to even greater underestimation of warm rain than in V6. Although there have been disputes on the convective-stratiform classification [Yuter and Houze, 1997; Atlas *et al.*, 1999, 2000], properties of the drop size spectra from the stratiform classification are consistent with the dominant growth processes of stratiform precipitation, which are vapor deposition onto existing ice particles and the collection of snow generated by the mesoscale updraft that develops in the upper levels in the stratiform regions with higher tops frequently seen in the western Pacific. However, the passage of the particles through the region of mesoscale updraft may not be sufficient for the growth of large drops in the stratiform regions with lower tops over the eastern Pacific. Thus stratiform rain over the eastern Pacific probably produces more small to medium size raindrops compared with the western Pacific, leading to underestimation of rain by the PR2A25 algorithm.

5. Summary and Conclusion

[28] The differences between PR2A25 [Iguchi *et al.*, 2000; Iguchi, 2007] and TMI2A12 [Kummerow *et al.*, 2001; Olson *et al.*, 2006] standard rainfall products over the eastern Pacific are well known [Berg *et al.*, 2002, 2006]. Rainfall for TMI2A12 is greater than for PR2A25 over the eastern Pacific, while the products are in good agreement over the western Pacific, and this results in different west-east gradients of rainfall. The GSMaP_TMI algorithm [Kubota *et al.*, 2007], which is a PR-consistent advanced microwave radiometer algorithm based on the study by Aonashi and Liu [2000], also gives rainfall greater than that given by the PR2A25 algorithm over the eastern Pacific, while the results are in good agreement over the western Pacific.

[29] Here, we have shown that discrepancies between TMI-observed TBs for the 19 GHz channel and those simulated from the PR rainfall estimates over the eastern Pacific are larger than those over the western Pacific, especially for rainfall in the lower to medium range (small attenuation). It is hypothesized that the DSDs of rainfall over the eastern Pacific have stronger maritimity (i.e., more small to medium sized raindrops) than the initial DSD model of PR2A25, representative of the “data-rich” western Pacific, leading to an underestimation of rain. The hypothesis is consistent with the convective ϵ from the α -adjustment procedure in the PR2A25 algorithm.

[30] A schematic illustration of precipitation features over the western and eastern Pacific is presented in Figure 7. There are large differences in the vertical structure of precipitation between the western and eastern Pacific. A larger population of warm rain and development of weak ice precipitation in convective rain are found in the eastern Pacific compared with the western Pacific, suggesting weaker updrafts [Zipser and Lutz, 1994]. Weaker updrafts help promote growth by coalescence by giving droplets more time to interact and advect less cloud water available for the growth of ice hydrometeors aloft. Similar to the convective rain, the development of weaker ice precipitation in stratiform rain is found over the eastern Pacific compared with the western Pacific. Active coalescence and less ice precipitation lead to DSDs with smaller median diameters [Rosenfeld and Ulbrich, 2003]. Thus the differences in the vertical structure of precipitation support the notion that the maritimity of DSDs is stronger for the eastern Pacific than for the western Pacific.

[31] Finally, we caution against using the present findings as quantitative validation of the passive algorithms (TMI2A12 and GSMaP_TMI) since other uncertainties remain.

[32] **Acknowledgments.** This study is supported by funding from the Japan Aerospace Exploration Agency/Earth Observation Research Center (JAXA/EORC) TRMM project and Japan Science and Technology (JST) Corporation, Core Research for Evolution Science and Technology (CREST). We wish to thank G. Liu from Florida State University for providing his RTM. We also thank K. Aonashi from the Meteorological Research Institute (MRI) for his kind guidance on using the RTM. Discussions with T. Iguchi and N. Takahashi from the National Institute of Information and Communications Technology (NICT), T. Kozu from Shimane University, and T. Nakazawa from the MRI are appreciated. We also thank C. Kummerow for providing the TMI2A12 V6 algorithm code. The authors thank three anonymous reviewers for their constructive comments. The TRMM products were provided by JAXA. ERA40 data were provided from the European Center for Medium-range Weather Forecasts (ECMWF). The CWV, LWP, sea surface wind, and sea surface temperature data set retrieved from the TMI was obtained from the Remote Sensing Systems website.

References

- Aonashi, K., and G. Liu (2000), Passive microwave precipitation retrievals using TMI during the baiu period of 1998. part I: Algorithm description and validation, *J. Appl. Meteorol.*, *39*, 2024–2037.
- Atlas, D., C. W. Ulbrich, F. D. Marks Jr., E. Amitai, and C. R. Williams (1999), Systematic variation of drop size and radar-rainfall relations, *J. Geophys. Res.*, *104*, 6155–6169.
- Atlas, D., C. W. Ulbrich, F. D. Marks Jr., R. A. Black, E. Amitai, P. T. Wills, and C. E. Samsury (2000), Partitioning tropical oceanic convective and stratiform rains by draft strength, *J. Geophys. Res.*, *105*, 2259–2267.
- Awaka, J., T. Iguchi, and K. Okamoto (2007), Rain type classification algorithm, in *Measuring Precipitation From Space - EURAINSAT and*

- the Future*, edited by V. Levizzani, P. Bauer, and F. J. Turk, pp. 213–224, Springer, New York.
- Bauer, P., L. Schanz, and L. Roberti (1998), Correction of three-dimensional effects for passive microwave remote sensing of convective clouds, *J. Appl. Meteorol.*, **37**, 1619–1632.
- Berg, W. K., C. Kummerow, and C. A. Morales (2002), Differences between east and west Pacific rainfall systems, *J. Clim.*, **15**, 3659–3672.
- Berg, W. K., T. L'Ecuyer, and C. Kummerow (2006), Rainfall climate regimes: The relationship of regional TRMM rainfall biases to the environment, *J. Appl. Meteorol.*, **45**, 434–454.
- Bringi, V. N., V. Chandrasekar, H. Hubbert, E. Gorgucci, W. L. Randeu, and M. Schoenhuber (2003), Rindrop size distribution in different climate regimes from disdrometer and dual-polarized radar analysis, *J. Atmos. Sci.*, **60**, 354–365.
- Chandrasekhar, V., W. Li, and B. Zafar (2005), Estimation of raindrop size distribution from spaceborne radar observations, *IEEE Trans. Geosci. Remote Sens.*, **43**, 1078–1086.
- Coppens, D., and Z. S. Haddad (2000), Effects of raindrop size distribution variations on microwave brightness temperature calculation, *J. Geophys. Res.*, **105**, 24,483–24,489.
- Curtis, S., and R. Adler (2000), ENSO indices based on patterns of satellite-derived precipitation, *J. Clim.*, **15**, 2786–2793.
- Feingold, G., and Z. Levin (1986), The lognormal fit of raindrop spectra from frontal convective clouds in Israel, *J. Appl. Meteorol.*, **25**, 1346–1363.
- Greco, M., W. S. Olson, and E. N. Anagnostou (2004), Retrieval of precipitation profiles from multiresolution, multifrequency active and passive microwave observations, *J. Appl. Meteorol.*, **43**, 562–575.
- Haddad, Z. S., E. A. Smith, C. Kummerow, T. Iguchi, M. L. Farrar, S. L. D. M. Alves, and W. S. Olson (1997), The TRMM day-1 radar/radiometer combined rain-profiling algorithm, *J. Meteorol. Soc. Jpn.*, **75**, 799–808.
- Hitschfeld, W., and J. Bordan (1954), Errors inherent in the radar measurement of rainfall at attenuating wavelengths, *J. Atmos. Sci.*, **11**, 58–67.
- Iguchi, T. (2007), Space-borne radar algorithms, in *Measuring Precipitation From Space - EURAINSAT and the Future*, edited by V. Levizzani, P. Bauer, and F. J. Turk, pp. 199–212, Springer, New York.
- Iguchi, T., and R. Meneghini (1994), Intercomparison of single-frequency methods for retrieving a vertical rain profile from airborne or spaceborne radar data, *J. Atmos. Oceanic Technol.*, **11**, 1507–1516.
- Iguchi, T., T. Kozu, R. Meneghini, J. Awaka, and K. Okamoto (2000), Rain-profiling algorithm for the TRMM precipitation radar, *J. Appl. Meteorol.*, **39**, 2038–2052.
- Janowiak, J. E., P. A. Arkin, P. Xie, M. Morrissey, and D. R. Legates (1995), An examination of the east Pacific ITCZ rainfall distribution, *J. Clim.*, **8**, 2810–2823.
- Kim, M.-J., J. A. Weinman, and R. A. Houze Jr. (2004), Validation of maritime rainfall retrievals from the TRMM microwave radiometer, *J. Appl. Meteorol.*, **43**, 847–859.
- Klaassen, W. (1990), Attenuation and reflection of radio waves by a melting layer of precipitation, *Proc. IEEE*, **137**, 39–44.
- Kozu, T., et al. (2001), Development of precipitation radar onboard the Tropical Rainfall Measuring Mission (TRMM) satellite, *IEEE Trans. Geosci. Remote Sens.*, **39**, 102–116.
- Kubota, T., et al. (2007), Global precipitation map using satelliteborne microwave radiometers by the GSMaP project: Production and validation, *IEEE Trans. Geosci. Remote Sens.*, **45**, 2259–2275.
- Kummerow, C., W. S. Olson, and L. Giglio (1996), A simplified scheme for obtaining precipitation and vertical hydrometeor profiles from passive microwave sensors, *IEEE Trans. Geosci. Remote Sens.*, **34**, 1213–1232.
- Kummerow, C., et al. (2000), The status of the Tropical Rainfall Measuring Mission (TRMM) after two years in orbit, *J. Appl. Meteorol.*, **39**, 1965–1982.
- Kummerow, C., et al. (2001), The evolution of the Goddard Profiling Algorithm (GPROF) for rainfall estimation from passive microwave sensors, *J. Appl. Meteorol.*, **40**, 1801–1820.
- Liu, G. (1998), A fast and accurate model for microwave radiance calculations, *J. Meteorol. Soc. Jpn.*, **76**, 335–343.
- Marshall, J. S., and W. M. Palmer (1948), The distribution of raindrops with size, *J. Atmos. Sci.*, **5**, 165–166.
- Meneghini, R., T. Iguchi, T. Kozu, L. Liao, K. Okamoto, J. A. Jones, and J. Kwiatkowski (2000), Use of the surface reference technique for path attenuation estimates from the TRMM precipitation radar, *J. Appl. Meteorol.*, 2053–2070.
- Okamoto, K. (2003), A short history of the TRMM precipitation radar, in *Cloud Systems, Hurricanes and the Tropical Rainfall Measurement Mission (TRMM): A Tribute to Dr. Joanne Simpson*, *Meteorol. Monogr.*, **51**, pp. 187–195, Am. Meteorol. Soc., Boston, Mass.
- Olson, W. S., et al. (2006), Precipitation and latent heating distributions from satellite passive microwave radiometry. part I: Improved method and uncertainty estimates, *J. Appl. Meteorol.*, **40**, 702–720.
- Petty, G. W. (1994), Physical retrievals of over-ocean rain rate from multichannel microwave imagery. part I: Theoretical characteristics of normalized polarization and scattering indices, *Meteorol. Atmos. Phys.*, **54**, 79–99.
- Robertson, F. R., D. E. Fitzjarrald, and C. D. Kummerow (2003), Effects of uncertainty in TRMM precipitation radar path integrated attenuation on interannual variations of tropical oceanic rainfall, *Geophys. Res. Lett.*, **30**(4), 1180, doi:10.1029/2002GL016416.
- Rosenfeld, D., and C. W. Ulbrich (2003), Cloud microphysical properties, process, and rainfall estimation opportunities, in *Radar and Atmospheric Science: A Collection of Essays in Honor of David Atlas*, *Meteorol. Monogr.*, **52**, pp. 237–258, Am. Meteorol. Soc., Boston, Mass.
- Sasaki, H., S. Shige, and K. Okamoto (2007), Improvements of brightness temperature simulations for validation of TRMM rainfall products (in Japanese), *J. Remote Sens. Soc. Jpn.*, **27**, 153–166.
- Schumacher, C., and R. A. Houze Jr. (2003), The TRMM precipitation radar's view of shallow, isolated rain, *J. Appl. Meteorol.*, **42**, 1519–1524.
- Sekhon, R. S., and R. C. Srivastava (1971), Doppler radar observations of drop size distributions in a thunderstorm, *J. Atmos. Sci.*, **28**, 983–994.
- Shige, S., H. Sasaki, K. Okamoto, and T. Iguchi (2006), Validation of rainfall estimates from the TRMM precipitation radar and microwave imager using a radiative transfer model: 1. Comparison of the version-5 and -6 products, *Geophys. Res. Lett.*, **33**, L13803, doi:10.1029/2006GL026350.
- Shige, S., Y. N. Takayabu, W.-K. Tao, and C.-L. Shie (2007), Spectral retrieval of latent heating profiles from TRMM PR data. part II: Algorithm improvement and heating estimates over tropical ocean regions, *J. Appl. Meteorol.*, **46**, 1098–1124.
- Shige, S., Y. N. Takayabu, and W.-K. Tao (2008), Spectral retrieval of latent heating profiles from TRMM PR data. part III: Estimating apparent moisture sink profiles over tropical oceans, *J. Appl. Meteorol.*, **47**, 620–640.
- Short, D. A., and K. Nakamura (2000), TRMM radar observations of shallow precipitation over the tropical oceans, *J. Clim.*, **13**, 4107–4124.
- Simpson, J., R. F. Adler, and G. R. North (1988), A proposed satellite Tropical Rainfall Measuring Mission (TRMM), *Bull. Am. Meteorol. Soc.*, **69**, 278–295.
- Simpson, J., C. Kummerow, W.-K. Tao, and R. F. Adler (1996), On the Tropical Rainfall Measuring Mission (TRMM), *Meteorol. Atmos. Phys.*, **60**, 19–36.
- Smith, E. A., and T. D. Hollis (2003), Performance evaluation of level-2 TRMM rain profile algorithms by intercomparison and hypothesis testing, in *Cloud Systems, Hurricanes and the Tropical Rainfall Measurement Mission (TRMM): A Tribute to Dr. Joanne Simpson*, *Meteorol. Monogr.*, **51**, pp. 207–222, Am. Meteorol. Soc., Boston, Mass.
- Stout, G. E., and E. A. Mueller (1968), Survey of relationships between rainfall rate and radar reflectivity in the measurement of precipitation, *J. Appl. Meteorol.*, **7**, 465–474.
- Takayabu, Y. N. (2002), Spectral representation of the rain features and diurnal variations observed with TRMM PR over the equatorial area, *Geophys. Res. Lett.*, **29**(12), 1584, doi:10.1029/2001GL014113.
- Tokay, A., and D. A. Short (1996), Evidence from tropical raindrop spectra of the origin of rain from stratiform versus convective clouds, *J. Appl. Meteorol.*, **35**, 355–371.
- Willis, P. T., and P. Tattelman (1989), Drop-size distributions associated with intense rainfall, *J. Appl. Meteorol.*, **28**, 3–15.
- Yang, S., W. Olson, J. J. Wang, T. L. Bell, E. A. Smith, and C. D. Kummerow (2006), Precipitation and latent heating distributions from satellite passive microwave radiometry. part II: Evaluation of estimates using independent data, *J. Appl. Meteorol.*, **45**, 721–739.
- Yuter, S. E., and R. A. Houze Jr. (1995), Three-dimensional kinematic and microphysical evolution of Florida cumulonimbus. part II: Frequency distribution of vertical velocity, reflectivity, and differential reflectivity, *Mon. Weather Rev.*, **123**, 1941–1963.
- Yuter, S. E., and R. A. Houze Jr. (1997), Measurements of raindrop size distributions over the Pacific warm pool and implications for Z-R relations, *J. Appl. Meteorol.*, **36**, 847–867.
- Yuter, S. E., and W. S. Parker (2001), Rainfall measurement on ship revisited: The 1997 PACS TEPPS cruise, *J. Appl. Meteorol.*, **40**, 1003–1018.
- Zipser, E. J., and K. R. Lutz (1994), The vertical profile of radar reflectivity of convective cells: A strong indicator of storm intensity and lightning probability?, *Mon. Weather Rev.*, **122**, 1751–1759.

S. Kida, K. Okamoto, H. Sasaki, S. Shige, and T. Watanabe, Department of Aerospace Engineering, Osaka Prefecture University, 1-1 Gakuen-cho, Sakai, Osaka 599-8531, Japan. (shige@aero.osakafu-u.ac.jp)

T. Kubota, Earth Observation Research Center, Japan Aerospace Exploration Agency, 2-1-1, Sengen, Tsukuba, Ibaraki 305-8505, Japan.